

Constructing Arbitrary Coherent Rearrangements in Optical Lattices

Alexander Roth,^{1,2} Liyang Qiu,¹ Timon Hilker,^{1,3} Titus Franz,^{1,4} and Philipp M. Preiss^{1,4,*}

¹*Max Planck Institute of Quantum Optics, Hans-Kopfermann-Str.1, Garching D-85748, Germany*

²*Fakultät für Physik, Ludwig-Maximilians-Universität, Schellingstr. 4, München D-80799, Germany*

³*Department of Physics and SUPA, University of Strathclyde, Glasgow G4 0NG, United Kingdom*

⁴*Munich Center for Quantum Science and Technology (MCQST), Schellingstr. 4, München D-80799, Germany*

(Dated: March 5, 2026)

Coherent control of motional degrees of freedom of ultracold atoms in optical lattices offers a promising route towards programmable quantum dynamics with massive particles. We propose and analyze a scheme for implementing coherent rearrangement of ultracold atoms, corresponding to arbitrary unitary transformations on single-particle motional states. Exploiting an analogy between dynamics in optical superlattices and discrete linear optics, we employ the Clements scheme to systematically construct any global N -dimensional single-particle unitary from tunneling and phase shifts in arrays of double wells. Tunneling is controlled globally, while local operations are achieved through site-resolved potential shifts. We numerically investigate the susceptibility of the scheme to intensity noise and addressing crosstalk. We identify key subroutines enabled by this unitary construction, including the Discrete Fourier Transform and the implementation of non-native Hamiltonians. Extending the scheme to two dimensions enables all-to-all atomic rearrangement with a circuit depth that scales sublinearly with the atom number, providing a high-density and highly scalable approach to atom rearrangement.

I. INTRODUCTION

The circuit description of quantum dynamics is a central pillar of quantum information science: Through a hierarchy of compilation levels, elementary operations can be combined into networks of gates that implement arbitrary unitary transformations [1, 2]. This abstraction separates quantum algorithms from the underlying experimental implementation and enables universal computation across a wide range of physical platforms. It also provides a systematic framework for decomposing complex dynamics into the experimentally most favorable building blocks on a given hardware architecture. For trapped ions and superconducting qubits, these building blocks correspond to finely tuned control pulses [3, 4], while in quantum optics they are realized by discrete physical optical elements [5–7].

A major open challenge is to extend this compilation-based approach to the dynamics of massive mobile particles. For ultracold atomic gases trapped in optical lattices, coherent quantum motion is driven by tunneling between neighboring sites. Together with collisional interactions, such tunneling dynamics enable highly coherent evolution of thousands of particles over hundreds of tunneling times, giving rise to strongly entangled motional states [8, 9]. Despite this high degree of coherence, control over cold-atom lattice dynamics is typically limited to global operations, such as temporal modulation of lattice depths or overall confining potentials, resulting in coarse-grained control.

Bringing together the coherence of atomic motion in optical lattices with the programmability of quantum cir-

cuit models opens new perspectives for quantum simulation and computation with itinerant particles. Discrete motional unitaries can be employed for state preparation [10] and for the emulation of imaginary-time evolution [11]. They further enable advanced measurement protocols based on collective interference [12, 13] or on the coherent rotation of single- and two-particle correlations into the measurement basis prior to site-resolved imaging [14–16]. Beyond quantum simulation, locally programmable motional unitaries form a key ingredient of recently proposed architectures for fermionic quantum computation [17, 18] and for error-correction schemes targeting motional degrees of freedom [19, 20].

In this article, we present a systematic framework for compiling arbitrary N -dimensional *single-particle* unitaries from sequences of experimentally realizable local gates. This decomposition is universal. It derives from an analogy between programmable multi-mode optical beam splitters and dynamics in optical superlattices [14, 21–23], where tunneling and potential shifting operations can be interpreted as beam splitter and phase-shift operations [5, 6]. Akin to the optical case, stroboscopic dynamics in optical superlattices can thus be programmed to transform single-particle quantum states spanning N input modes into arbitrary N output modes. The operation acts on single-particle motional modes in the motional ground band only and is decoupled from the particles’ internal degrees of freedom. It is thus applicable to bosons and fermions in optical lattices. Experimentally, our scheme requires only globally controlled tunneling in a superlattice and local phase-shifting operations [14].

We highlight two key anticipated applications of the method. First, the scheme will enable the synthesis of specific unitaries as subroutines of quantum simulation approaches. We demonstrate how to engineer unitaries generated by Hamiltonians with non-native terms, such

* philipp.preiss@mpq.mpg.de

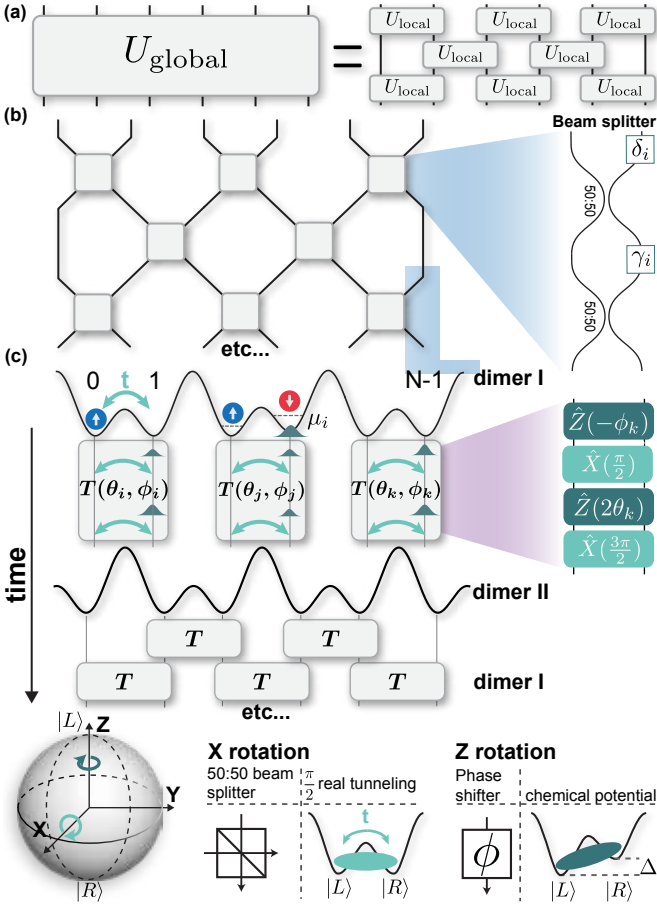


FIG. 1. **Parallels of Quantum Optics and Optical Lattices.** (a) An arbitrary global unitary U_{global} is systematically constructed from local two-mode unitary gates U_{local} . (b) An optical interferometer constructed using the Clements scheme realizes arbitrary N -mode transformations using brick-wall lattices of generalized beam splitters. The inset shows a single two-mode operation composed of two 50:50 beam splitters and phase shifters applying phases γ and δ . (c) Atomic dynamics between discrete modes in optical superlattices can be constructed by analogy to optical interferometers. An \hat{X} rotation (beam splitter) is performed by enabling tunneling, while a \hat{Z} rotation (phase shifter) is performed by applying a local energy offset μ_i . The brick-wall structure is realized by alternating the superlattice dimerization between dimer I and dimer II, which is achieved by adjusting the superlattice phase. In each time step, a two-mode transformation $T(\theta_i, \phi_i)$ is implemented in parallel on all dimers of the current dimerization through a sequence of native \hat{X} and \hat{Z} gates.

as long-range tunneling, and detail the realization of the Discrete Fourier Transform (DFT) as a gate sequence in a lattice. The DFT is a primitive for many quantum algorithms and will find important applications as a coherent mapping between position and momentum space, enabling momentum space microscopy and many-body interference experiments [12, 13, 24]. Second, we show that our approach can realize swap networks where all

particles in a system perform permutations simultaneously. Applying this approach to atom rearrangement in two-dimensional $N = L \times L$ arrays, we demonstrate a scheme by which atoms in $\mathcal{O}(N)$ modes can be rearranged with all-to-all connectivity in an $\mathcal{O}(\sqrt{N})$ depth circuit. The sublinear scaling of the depth of the circuit presents a significant scaling advantage over serial, tweezer-based sorting approaches [25].

II. SUPERLATTICE ARCHITECTURE AND OPTICAL ANALOGY

A. Physical Platform and Motional Gates

We seek to construct motional unitaries driven by tunneling dynamics in optical superlattices. Such lattices are formed by superimposing two lattices with different periodicities with dynamical control over their depths and relative spatial phases. This architecture realizes large-scale arrays of double-wells with finely tunable local potential geometries [14, 23, 26]. The exquisite control over dynamics within each local motif has led to powerful applications, including the realization of higher-order tunneling processes, collisional entangling gates, and local state manipulation [14, 21, 27–31].

To establish a correspondence between optical interferometers and atoms in optical superlattices, we consider cold atoms trapped in the lowest band of a one-dimensional optical superlattice with N modes as shown in Fig. 1c. We assume a spinless gas (with the extension to several internal states being straightforward) and the non-interacting limit. The superlattice creates an array of double-well potentials with globally tunable geometry. In particular, the dimerization of the superlattice can be switched between odd and even by dynamically adjusting the relative spatial phase between the short and the long lattice [21]. Each double-well forms a natural two-level system, or motional qubit, where the atom's position in the left $|L\rangle$ or right $|R\rangle$ well defines the computational basis. Full motional qubit control is achieved via two native operations: controlling the tunneling amplitude (t) to perform \hat{X} -rotations, and applying an energy offset Δ for \hat{Z} -rotations. Together, these form a universal set for any local $SU(2)$ operation on a single qubit [17, 18]. Both gates have already been demonstrated experimentally [14, 24]. The native $\hat{X}(\alpha)$ and $\hat{Z}(\theta)$ rotations are defined as:

$$\hat{X}(\alpha) = \begin{pmatrix} \cos(\frac{\alpha}{2}) & -i \sin(\frac{\alpha}{2}) \\ -i \sin(\frac{\alpha}{2}) & \cos(\frac{\alpha}{2}) \end{pmatrix}; \quad \hat{Z}(\theta) = \text{diag}(1, e^{i\theta}). \quad (1)$$

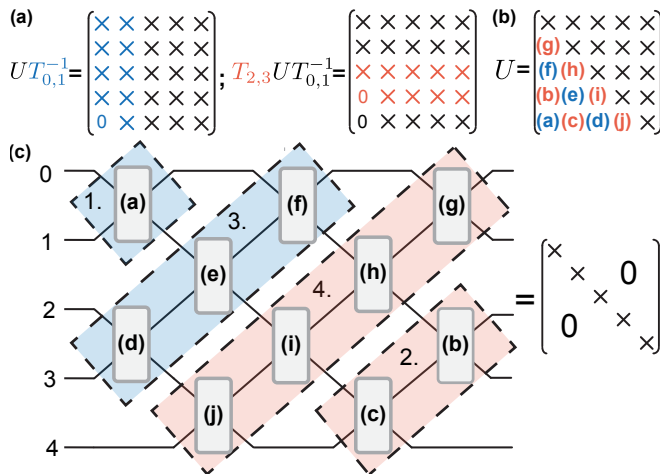


FIG. 2. **Clements Scheme.** (a) A Givens rotation multiplied from the right (left) mixes two columns (rows) to eliminate a specific target element of an arbitrary unitary U . A multiplication from the right (left) is colored in blue (red). (b) The Clements scheme transforms a unitary into a diagonal matrix by eliminating the sub diagonal elements in a “snake-like” pattern, alternating between left and right multiplied Givens rotations. (c) The physical brick-wall circuit that implements the decomposition. Each rectangular gate corresponds to a single Givens rotation $T_{n,m}(\theta, \phi)$ used to nullify one element in panel (b). The different sections correspond to the subdiagonals of U .

B. Unitary Decomposition via the Clements Scheme

To construct an arbitrary single-particle N -dimensional unitary transformation using only operations naturally available in a superlattice architecture, namely local \hat{X} and \hat{Z} operations, we leverage an analogy with linear optics, specifically the decomposition scheme developed by Clements et al. [6]. The Clements decomposition is widely used in linear optics to implement programmable multimode interferometers [32] that enable applications ranging from photonic quantum computing [33] and machine learning [34] to reconfigurable microwave photonics [35]. Its key advantages are that it uses the minimal number of two-mode gates, $N(N-1)/2$, and achieves the minimal possible circuit depth of N .

Following the Clements scheme [6], the full unitary $U = \sum_{i=0}^{N-1} |\phi_i\rangle\langle\psi_i|$, which maps an initial orthonormal basis $\{|\psi_i\rangle\}$ onto a desired output basis $\{|\phi_i\rangle\}$, is constructed as a product of two-mode transformations, each acting on a two-dimensional subspace spanned by sites n

and m

$$T_{n,m}(\theta, \phi) = \begin{pmatrix} \ddots & & & & \\ & 1 & & & \\ & e^{i\phi} \cos \theta & -\sin \theta & & \\ & e^{i\phi} \sin \theta & \cos \theta & & \\ & & & 1 & \\ & & & & \ddots \end{pmatrix}_{N \times N} \quad (2)$$

and a diagonal phase matrix, D :

$$U(N) = D \left(\prod_{(n,m) \in S} T_{n,m} \right). \quad (3)$$

S denotes the ordered set of adjacent two-mode transformations. This procedure is closely analogous to a QR decomposition in linear algebra, where successive orthogonal (or unitary) transformations are applied to zero out sub-diagonal elements of a matrix. In the Clements scheme, each two-mode operation $T_{n,m}$ plays the role of a localized Givens rotation that removes a specific off-diagonal element of the evolving unitary, as illustrated in Fig.2. Starting from the bottom-left corner, the algorithm sweeps through the sub-diagonals in a “snake-like” pattern: moving upward along one sub-diagonal, then downward along the next, nullifying one element at a time until the matrix becomes upper-triangular. Because U is unitary, the resulting upper-triangular matrix must be diagonal. A full derivation is given in Clements et al. [6].

In optical networks, $T_{n,m}$ represents a generalized two-mode beam splitter, which can physically be realized with two balanced beam splitters and two local phase shifters. To implement $T_{n,m}$ in a superlattice architecture, each transformation is realized using a four-gate $Z_2 X_2$ sequence (derived in Appendix A),

$$T_{n,m}(\theta, \phi) = e^{i(\phi-\theta+\pi)} \hat{X} \left(\frac{3\pi}{2} \right) \cdot \hat{Z}(2\theta) \cdot \hat{X} \left(\frac{\pi}{2} \right) \cdot \hat{Z}(-\phi) \quad (4)$$

The global phase accounts for the conversion from $U(2)$ to $SU(2)$ and for the phase offset between symmetric and asymmetric \hat{Z} gates. The phase can, however, be absorbed by the diagonal phase matrix D by finding new angles $\{\theta', \phi'\}$ (see Appendix B). We will omit the prime in the following.

As illustrated in Fig. 1c, this sequence maps directly onto timed control pulses. Crucially, all \hat{X} -rotations in a given layer require the same rotation angle of $\pi/2$ or $3\pi/2$, meaning that all tunnel pulses can be carried out in parallel and via global control of the tunneling t for a specific duration. Only the \hat{Z} -rotations are achieved by applying local energy offsets Δ provided by local addressing beams. Arbitrary local motional unitaries thus require local control over on-site phase shifts only. This architecture is inherently scalable and significantly more robust than any scheme requiring direct local control of the

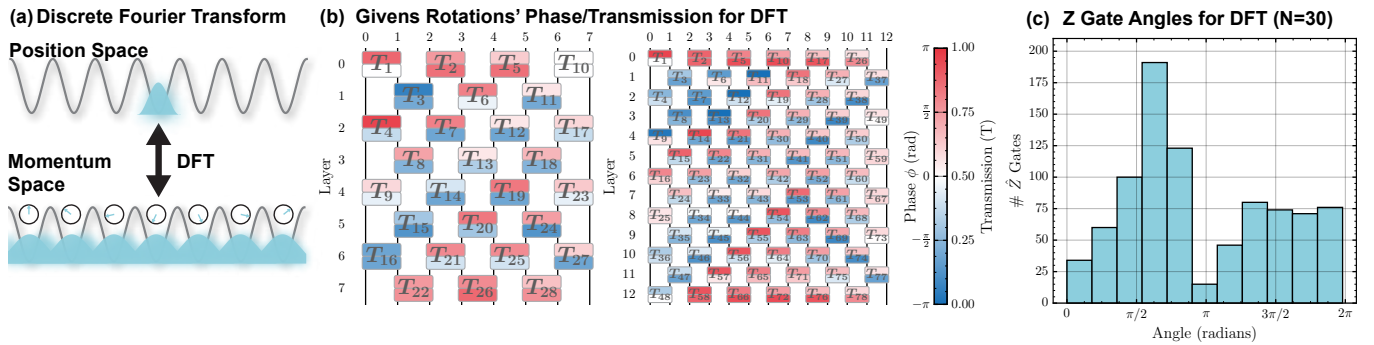


FIG. 3. **Decomposition Details of a DFT.** (a) A single particle, initially localized at a specific site (a position eigenstate), is coherently transformed into a delocalized state with a periodic phase structure across the entire array (a momentum eigenstate). (b) The circuit decomposition of the DFT unitary for $N = 8$ (left) and $N = 13$ (right) systems. Each colored rectangle represents a two-mode gate. The upper rectangle indicates the gate's phase ϕ , while the lower rectangle represents its transmission probability, $T = \cos^2(\theta)$. A translational pattern emerges for odd N . (c) Histogram of the required \hat{Z} gate rotation angles for an $N = 30$ DFT, showing that angles are distributed across the full $[0, 2\pi]$ range.

tunnel coupling t . We note that related control strategies have been proposed and demonstrated for discrete time quantum walks in spin-dependent optical lattices [36].

III. APPLICATIONS OF UNITARY CONTROL

Programmable motional unitaries of non-interacting particles in optical lattices may serve as initialization or readout tools and constitute important subroutines for information processing with itinerant particles [17, 18, 20]. Of the many possible applications, we discuss two specific instances in this section: the Discrete Fourier Transform (DFT) and the implementation of non-native Hamiltonians.

A. Discrete Fourier Transformation

Accessing momentum-space observables is paramount for characterizing a wide range of quantum many-body phenomena, from probing band structure and spectral functions to identifying quantum phase transitions and pairing correlations [37–40].

The established procedure for probing optical lattice systems in momentum space is time-of-flight imaging, for which lattices are switched off suddenly and particles are detected in free space or in a pinning lattice after ballistic propagation, revealing momentum space densities and correlations [39, 40]. The time-of-flight operation itself is incoherent, in the sense that performing the inverse operation is impractical and particles are usually not in a lowest-band lattice mode after expansion [39].

In contrast, we now consider the unitary Discrete Fourier Transform in an optical lattice. The DFT acts only within the lowest band of an optical lattice and preserves coherences between motional states. Its important features include: 1) Its fully coherent nature, allowing

for coherent evolution between position and momentum space and vice-versa; 2) Its use as a subroutine for quantum algorithms, for example collective measurements on multiple system copies [12, 13, 24]; 3) The mapping of N discrete lattice momentum modes to N spatial modes, enabling single-shot readout of lattice momentum in quantum gas microscopes. Approximate schemes for a lattice DFT have been proposed [41], but we are not aware of other exact lattice implementations.

The matrix elements of a DFT can be written in the following way:

$$\text{DFT} = \frac{1}{\sqrt{N}} \sum_{j,k=0}^{N-1} \omega^{jk} |k\rangle \langle j| \quad (5)$$

where $\omega = e^{2\pi i/N}$ is a primitive N -th root of unity [42]. In all discussions and figures, this matrix is additionally shifted, so that the zero-momentum component is centered, analogous to the *fftshift*.

Figure 3b shows the phase and the transmission probability (ϕ and $T = \cos^2(\theta)$) for the $T_{n,m}(\theta, \phi)$ of the decomposed DFTs for two system sizes. A pattern emerges for T resulting from the reflection at the boundaries of the array.

The Discrete Fourier Transform implemented coherently in the lattice offers a plethora of new experimental capabilities. Its unitary nature can, for example, be used for the manipulation of specific momentum states by mapping from position space to momentum space, performing a local operation, and mapping back to position space. For fermionic many-body systems, where entropy in thermal states is concentrated in specific regions of the Brillouin zone, a single application of the DFT also localizes entropy spatially, which may enable novel cooling methods based on removing the most entropic momentum states from a system.

Beyond the standard DFT, the decomposition framework can naturally be extended to implement the Dis-

crete Fractional Fourier Transformation (FrFT), a unitary definition of which is provided in [43]. The FrFT generalizes the Fourier transform as a rotation in phase space that can prepare and measure states in a continuous set of complementary bases interpolating between position and momentum space.

The one-dimensional DFT can be straightforwardly extended to two (or higher) dimensions by exploiting its separability. In two dimensions, this allows one to first apply a one-dimensional DFT simultaneously to all columns, followed by a one-dimensional DFT applied to all rows. Each of these one-dimensional DFTs has depth $\mathcal{O}(L)$, resulting in a total circuit depth of $\mathcal{O}(\sqrt{N})$, where we adopt the notation $N = L \times L$ with L denoting the lattice size. We will retain this notation in the two-dimensional analysis, using N to represent the total number of modes.

B. Simulating Non-Native Hamiltonians

An important application of our decomposition framework is the simulation of Hamiltonians with non-native unitary dynamics $\hat{U}(\tau) = \exp(-i\hat{H}\tau/\hbar)$. As a demonstration, we construct the circuits implementing two such unitaries, the detailed decomposition schemes of which are provided in Figure 4. First, we implement a fast scrambling Hamiltonian with non-local, tree-like tunnel couplings, a model connected to studies of quantum chaos and the black hole information paradox [44]. Second, we consider a Hamiltonian with next-nearest-neighbor (NNN) hopping, representing a Hubbard model beyond the tight-binding limit.

IV. ATOM REARRANGEMENT

A key ingredient of the recent successes of quantum information science with neutral atoms is the ability to dynamically reconfigure atoms in optical trap arrays [25]. This capability enables the deterministic assembly of atomic registers from stochastically loaded arrays as a starting point for quantum many-body physics or quantum computation [45–48]. In this context, a specific initial configuration is converted into a target configuration, although it is immaterial which atom is moved to a specific target site, granting some freedom in the design of the best routing path. A more challenging situation arises for coherent mid-circuit rearrangement, as has been used for logical gates in zoned computing architectures [49]. Here, atoms have to be moved from specific initial to specific target sites while maintaining possible entanglement to static atoms in order to enable the desired computational connectivity. In all cases, rearrangement operations typically move individual or blocks of atoms in mobile tweezers and are carried out serially [25]. Parallelized, constant-time protocols have recently been demonstrated for short-range atom rearrangement [50].

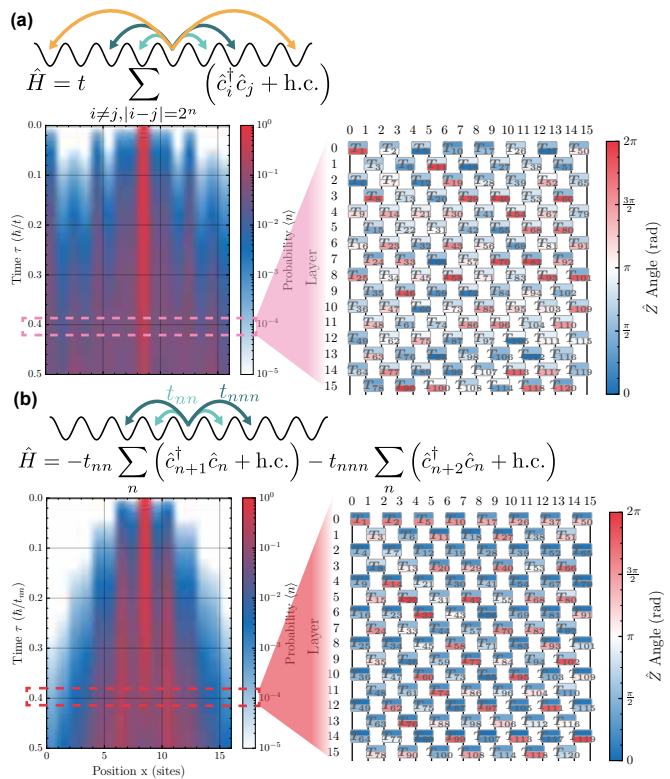


FIG. 4. Simulating Non-Native Hamiltonian Dynamics. The framework can simulate dynamics not natively generated by the hardware by decomposing the time-evolution operator $\hat{U}(\tau) = e^{-i\hat{H}\tau/\hbar}$ into a local gate sequence. We show the time evolution of a particle initially localized in the center of a 16-site array (left panels) and the corresponding circuit decomposition of the unitary operator for a given time τ (right panels). (a) Evolution under a fast scrambling Hamiltonian with non-local, tree-like interactions as described in [44]. The particle’s probability rapidly spreads across the system. (b) Evolution under a Hamiltonian with nearest-neighbor (NN) and next-nearest-neighbor (NNN) hopping ($\frac{t_{n,nn}}{t_{nn}} = 2$) beyond the tight-binding approximation.

The scheme we outline here can be used to perform atom rearrangement using coherent ground band dynamics in optical lattices instead. As we demonstrate below, this gives rise to an appealing alternative paradigm for parallelized two-dimensional atom reconfiguration, where the total depth of the rearrangement circuit is sublinear in the number of atoms to be transported.

The principal ingredient of the coherent rearrangement methods is shown in Figure 5a. For specific phase angles, the beam splitter unitary from Eq. 4 realizes transport primitives in each double-well — the identity $\hat{\mathbb{I}}$ for $\{\theta, \phi\} = \{0, 0\}$ and the $\widehat{\text{SWAP}}$ for $\{\theta, \phi\} = \{\frac{3\pi}{2}, \pi\}$. These circuits can be combined to form SWAP networks to rearrange atoms in one dimension, as is routinely done in quantum computing architectures with local connectivity [51, 52]. Owing to the parallel implementation of $\hat{\mathbb{I}}$ and $\widehat{\text{SWAP}}$ gates in optical superlattices, a brick-wall cir-

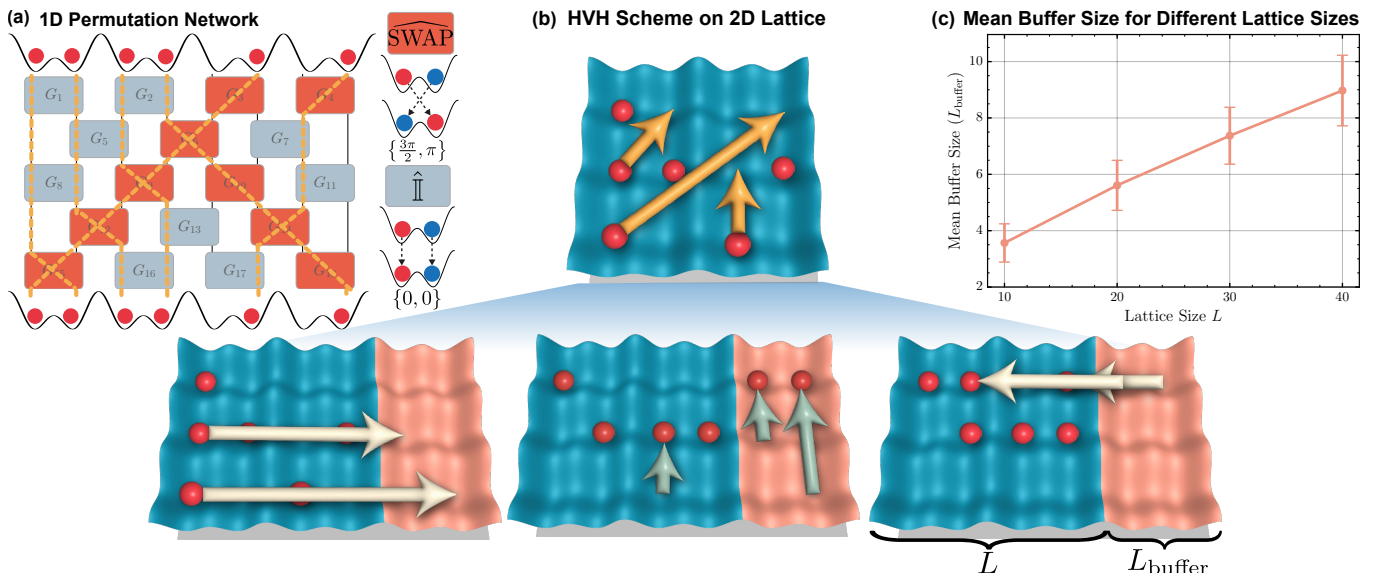


FIG. 5. **Atom Rearrangement in 1D and 2D** (a) A 1D permutation is decomposed into a network of two-site gates that either swap modes (red) or apply the Identity (gray). A $\overline{\text{SWAP}}$ gate is realized by setting $\{\theta, \phi\} = \{\frac{3\pi}{2}, \pi\}$ while the Identity $\hat{\mathbb{I}}$ is realized through $\{\theta, \phi\} = \{0, 0\}$ in Eq. 4. (b) The "Horizontal-Vertical-Horizontal" (HVH) scheme is used for conflict-free 2D atom rearrangement. The three steps are: (1) a horizontal sort moves atoms into a temporary buffer region (orange); (2) a vertical sort places atoms in their correct target rows; and (3) a final horizontal placement moves them into the desired target columns. (c) We show the mean buffer size L_{buffer} required to generate a conflict-free rearrangement using the HVH scheme for an $L \times L$ fully filled lattice. Each data point is the average over 100,000 random target configurations, with error bars indicating the standard deviation. The points are connected as a guide to the eye. The worst possible buffer size needed is $L - 1$ although this is rarely the case.

cuit of depth N can perform arbitrary, one-dimensional, parallel rearrangement of atoms in N modes.

Extending the parallel lattice swap network to two dimensions enables the implementation of arbitrary permutation matrices on an $L \times L$ lattice. However, avoiding configurations where two atoms simultaneously occupy the same lattice site requires careful scheduling of the individual moves. To this end, we introduce the "Horizontal-Vertical-Horizontal" (HVH) scheme shown in Figure 5b which decomposes the 2D problem into three sequential 1D permutations: a conflict-resolving horizontal pass, a vertical sorting pass, and a final horizontal placement. In the first horizontal permutation, atoms in each row are moved from their starting positions (r_S, c_S) to intermediate positions (r_S, c_I) chosen such that the subsequent vertical permutation is conflict-free, i.e., no two atoms in the same column are routed to the same target row. To achieve this, the available columns are extended from the original L columns to $L_{\text{ext}} = L + L_{\text{buffer}}$. In the vertical permutation, all atoms are then shifted to their respective target rows r_T . Finally, during the second horizontal permutation, atoms are placed in their target columns, reaching their final positions (r_T, c_T) .

This approach guarantees conflict-free routing for arbitrary permutations in two dimensions, provided enough buffer columns are available. The worst-case scenario requires $L - 1$ buffer columns. This makes the total width L_{ext} at worst $2L - 1$. We explore the typical buffer size re-

quired by simulating random all-to-all permutations on an $L \times L$ array. Figure 5c shows the mean buffer size needed for conflict-free rearrangement for different lattice sizes $L \times L$, demonstrating that typically required buffer sizes are much smaller than the maximum of $L - 1$ auxiliary columns. The latter is needed exponentially rarely, even for a fully filled lattice. The plot was generated by implementing a greedy algorithm for determining the movements of the atoms.

The HVH scheme thus decomposes the rearrangement of L^2 modes into two sequential horizontal permutations of depth $\mathcal{O}(2L)$ and a vertical permutation of depth $\mathcal{O}(L)$, resulting in a total circuit depth of $\mathcal{O}(5L)$ for the two-dimensional reconfiguration. This corresponds to a sublinear scaling in the total system size $N = L^2$, namely $\mathcal{O}(\sqrt{N})$. Compared to the serial rearrangement typically employed in tweezer arrays, which takes at least $\mathcal{O}(N)$ moves [49, 53, 54], the HVH approach is markedly more efficient.

We note that for specific instances of the rearrangement problem, more efficient circuits than the HVH scheme are possible. In the most general case of N distinguishable particles, $N!$ rearrangements are possible. Therefore, the number of gates required scales as $\mathcal{O}(\log_2(N!)) \approx \mathcal{O}(N \log_2(N))$ using Stirling's approximation. The HVH scheme, on the other hand, requires $\mathcal{O}(3N\sqrt{N})$ gates.

The coherent rearrangement scheme allows any atom

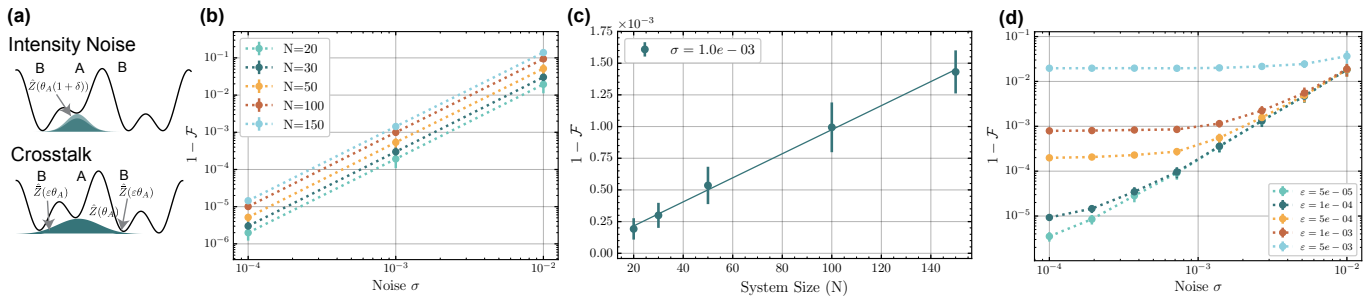


FIG. 6. **Error Analysis for DFT Matrix.** Performance under two primary noise channels: random multiplicative noise on local gate angles and correlated crosstalk errors from addressing beams. The infidelity, defined as $1 - \mathcal{F}$ where $\mathcal{F} = |\langle \psi_{\text{ideal}} | \psi_{\text{noisy}} \rangle|^2$ is the state fidelity per mode, is used as the error metric. (a) Top: Intensity fluctuations in the addressing beams result in random multiplicative phase noise on the local \hat{Z} gates. Bottom: A crosstalk error occurs when an addressing beam on A affects the neighboring sites B which results in a slight tilt of the neighboring double-well. This effectively introduces a $\hat{Z}(\varepsilon\theta_A) \equiv \text{diag}(e^{i\varepsilon\theta_A}, 1)$ gate on the neighboring sites B where ε is the crosstalk strength. (b) Infidelity as a function of multiplicative noise strength σ for various system sizes N . Each point is the average over 100 random input states and 100 noise instances. Dotted lines are guides for the eye connecting the data points. (c) Fidelity versus system size N for a fixed noise strength of $\sigma = 10^{-3}$. The solid line represents a linear fit to the data, demonstrating that the infidelity scales linearly with N . (d) Infidelity versus noise strength σ in the presence of crosstalk error ε (for $N = 20$). For large crosstalk ($\varepsilon \geq 5 \times 10^{-4}$), a fidelity floor appears, limiting performance regardless of the intrinsic noise σ . Dotted lines are guides for the eye. Error bars denote the standard deviation.

to be moved to any site on demand, enabling all-to-all connectivity in optical lattice systems. Such dynamic reconfigurability is essential for a wide range of advanced quantum protocols, from implementing non-native couplings in quantum annealing [55] to generating large-scale cluster states for measurement-based quantum computing [56]. It also represents a critical capability for fault-tolerant architectures, where qubits must be dynamically rearranged for logical gate operations and error correction [49].

Our approach exhibits a fundamentally different error behavior than tweezer-based transport. The latter places atoms at the correct target site with high fidelity, but often introduces motional excitations to higher bands, requiring additional cooling after transport [25, 46, 47, 49]. In contrast, the coherent rearrangement protocol involves only lowest-band dynamics. Phase errors may cause atoms to occupy incorrect sites (see next section for a detailed error analysis), but they remain in the ground band. This error channel can be advantageous for architectures relying on collisional interactions.

Compared to tweezer-based atomic rearrangement, for which atom spacings are typically several μm [25, 49], the coherent rearrangement in tunnel-coupled lattices can support much higher densities of order one particle per μm^2 . This provides interesting perspectives for neutral atom quantum computing architectures, for which it is desirable to place many atomic qubits in the field of view of a high-NA objective [48]. High-density coherent rearrangement can significantly enhance the number of atoms that can be stored in a given register area. One can also readily imagine hybrid tweezer-lattice architectures, where mobile tweezers transport atoms over large distances between landing zones, around which atoms are

rearranged block-wise in high-density lattice arrays via the coherent rearrangement presented here. Similar considerations apply to the atom-by-atom assembly of Hubbard systems in optical lattices, where one of the central technical challenges is the placement of atoms in lattices at sub- μm scales [46, 47].

V. ERROR ANALYSIS

The realization of programmable global unitaries depends on the precision of the global tunneling \hat{X} and local phase shift \hat{Z} gates. Below we numerically investigate the precision required on individual gates to realize relevant applications.

The tunneling operations \hat{X} can be realized by global control of superlattice parameters, which can result in very high stabilities and accuracies of the desired gates [21, 23, 30]. The local phase shifting \hat{Z} is much more delicate, as it relies on high-resolution optics and precise alignment between addressing beams and optical lattices. We therefore assume the \hat{X} gates to be error-free and focus on errors in phase angles imprinted in the local \hat{Z} gates.

We investigate two primary error channels: random multiplicative noise and correlated crosstalk affecting neighboring qubits.

For benchmarking the algorithm's robustness, the target is to understand the noise levels permissible to achieve a high fidelity. For concreteness, we target an infidelity $1 - \mathcal{F} < 10^{-3}$, where $\mathcal{F} = |\langle \psi_{\text{ideal}} | \psi_{\text{noisy}} \rangle|^2$ is the state fidelity per mode.

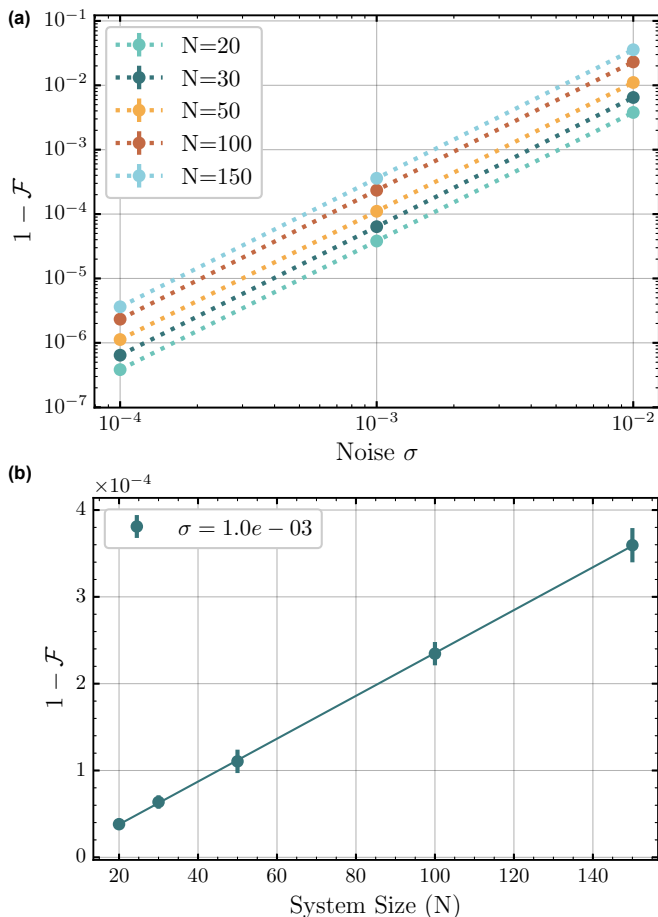


FIG. 7. **Error Analysis for Atom Rearrangement.** (a) The fidelity was averaged over 50 random permutation matrices, each tested with 50 random initial states and 50 noise instances. The fidelity is considerably higher compared to the DFT. (b) The fidelity decreases linearly with system size. A linear fit was applied.

A. Random Noise

We first model imperfections in gate calibration as a multiplicative error on the target rotation angle θ_0 . The actually implemented angle θ is given by:

$$\theta = \theta_0(1 + \delta)$$

where δ is a random variable drawn from the Gaussian distribution with standard deviation σ ($\delta \in \mathcal{N}(0, \sigma^2)$) for each application of the gate. This type of error corresponds to pointing fluctuations between the optical lattice and addressing optics or to power fluctuations in the addressing beams.

Figure 6b shows the infidelity for implementing a DFT under this noise model. The fidelity has a power-law behavior, as seen in Figures 6b-d, and can be fitted using

$$1 - \mathcal{F} = CN^k \sigma^b. \quad (6)$$

From Figure 6c, a linear behavior with N can be seen, therefore, $k = 1$. For the DFT, b was found to be

$b = 2.000 \pm 0.001$ and $C = 9.908 \pm 0.010$. This quadratic dependence on σ arises because for an arbitrary angle θ , the error term in the unitary $\exp(i\theta(1 + \delta))$ is first-order in δ , which leads to a second-order contribution to the state fidelity.

Atom rearrangement protocols also exhibit an infidelity that scales quadratically with noise ($b = 2.000 \pm 0.003$), yet they are substantially more robust than DFTs, with a smaller error coefficient of $C = 2.20 \pm 0.05$ (see Figure 7). This resilience is a direct consequence of the gate-level decomposition. Permutation matrices are constructed only from $\widehat{\text{SWAP}}$ and identity ($\widehat{\mathbb{I}}$) gates. In our multiplicative noise model, identity operations are intrinsically error-free (the angles are $\{0, 0\}$). Therefore, only the $\widehat{\text{SWAP}}$ gates contribute to the final infidelity.

B. Correlated Errors

A second major error source is optical crosstalk, where addressing a target site unintentionally affects its neighbors. Errors of this type occur if the intensity of the addressing beam is not fully localized to a single lattice site.

We model this crosstalk by assuming that a $\hat{Z}(\theta_A)$ gate, intended for site A, simultaneously induces an unwanted rotation $\hat{Z}(\varepsilon\theta_A)$ on each neighboring site B (Figure 6a). Here, ε is the dimensionless crosstalk strength. Consequently, the total rotation experienced by site B is a combination of its own noisy gate and the leakage from A. To simulate this error, we introduce a new gate $\hat{\hat{Z}}(\theta) \equiv \text{diag}(e^{i\theta}, 1)$. This gate only acts on the site B. The resulting operation on site B is given by:

$$\hat{\hat{Z}}_{\text{final}}(\theta_B) = \hat{\hat{Z}}(\varepsilon\theta_{A_1} + \varepsilon\theta_{A_2}) \quad (7)$$

where $\theta_{A_{1,2}}$ is the angle of the \hat{Z} gate on the two neighboring sites A_1 and A_2 . Since the beam profile of a laser beam can be modeled as Gaussian, the model only considers nearest-neighbor crosstalk.

Figure 6d investigates the impact of this correlated crosstalk error on the fidelity by implementing a DFT for a system size of $N = 10$. From the diagram, it is clear that ε has to be smaller than $1 \cdot 10^{-3}$ to reach a fidelity of $1 - \mathcal{F} < 10^{-3}$. For larger system sizes, the crosstalk error will have to decrease to even smaller values. Achieving such low crosstalk is one of the major experimental challenges of our scheme.

VI. DISCUSSION

In this work, we present a framework for decomposing arbitrary N -dimensional single-particle motional unitaries into native local gates for quantum simulators based on optical superlattices. By translating techniques

from multiport interferometry, our method provides a practical and efficient path to programming atomic dynamics in optical lattices. We show that this framework can realize essential 1D primitives such as the Discrete Fourier Transform and all-to-all atom rearrangement. Extending these ideas to two-dimensional systems with auxiliary sites, we propose a highly favorable rearrangement protocol with $\mathcal{O}(\sqrt{N})$ circuit depth that quadratically outperforms naive serial approaches. Our error analysis establishes practical performance thresholds for experiments based on globally controlled tunneling and locally controlled potential bias.

We emphasize that the scheme derives from *linear* optics and applies to non-interacting particles. The presence of interactions during the evolution would break the analogy to linear optics and require a much more complex description of the many-body dynamics.

Our approach describes the unitary transformation of a set of single-particle modes that remain orthogonal throughout their evolution [5, 6]. These transformations are independent of the nature of the particles occupying the modes. In particular, the scheme is not affected by Pauli blocking and applies to bosons and fermions. The statistics of the underlying particles only play a role in the number correlations observed at the output, in close analogy to optical many-body interferometers and boson sampling [57].

The correspondence between lattice dynamics and interferometers may be further expanded upon by using even more compact gate fabrics [58, 59] or by decomposing atomic dynamics into building blocks of larger size [60, 61]. Looking ahead, our framework opens the door for the programmable many-body interference of bosonic and fermionic ultracold atoms [46, 62]. It further provides a direct path towards momentum-space microscopy, where unitary transformation between momentum and position space enable the manipulation and readout of individual momentum modes. The scheme also enables probes of long-range coherence and pairing correlations [15, 16], for example in fermionic gases with momentum-space pairing signatures [40]. Finally, the ability to implement tailored unitary maps allows for the simulation of non-local Hamiltonians and quantum walks on arbitrary graphs [63].

ACKNOWLEDGMENTS

We acknowledge helpful conversations with Andrea Alberti, Immanuel Bloch, Robert Ott, Hannes Pichler, Torsten Zache, Johannes Zeiher and the FermiQP Team. This work was supported by the Max Planck Society (MPG), the German Federal Ministry of Research, Technology and Space (BMFTR grant agreement 13N15890, FermiQP), Germany's Excellence Strategy (EXC-2111-390814868) and the European Union's Horizon 2020 research and innovation program (grant agreements No 948240 — ERC

Starting Grant UniRand — and No 101212809 — ERC Proof of Concept FermiChem) and the Horizon Europe program HORIZON-CL4-2022 QUANTUM-02-SGA (project 101113690, PASQuans2.1). T.H. received funding from the European Research Council (ERC) under the European Union's Horizon Europe research and innovation program (Grant Agreement No 101165353 — ERC Starting Grant FOrbQ).

DATA AVAILABILITY

The data that support the findings of this article are openly available [64].

Appendix A: Derivation of ZXZX Angles from ZYZ Euler Angles

We aim to transform an arbitrary $U(2)$ operation, expressed in ZYZ Euler angle decomposition form as

$$\hat{U}_{YZZ} = e^{i\tilde{\alpha}} \hat{Z}(\beta) \hat{Y}(\gamma) \hat{Z}(\delta), \quad (\text{A1})$$

with $e^{i\alpha} \hat{U}_{YZZ} \in SU(2)$ into the ZXZX sequence form

$$\hat{U}_{ZXZX} = e^{i\alpha} \hat{X}(\frac{3\pi}{2}) \hat{Z}(\gamma) \hat{X}(\frac{\pi}{2}) \hat{Z}(\delta). \quad (\text{A2})$$

The symmetric \hat{Z} -gate, $\hat{Z}_{sym}(\theta) = \text{diag}(e^{-i\theta/2}, e^{i\theta/2})$, will be used (which differs only by a global phase from the asymmetric version).

We use the following identity for decomposing a Y -rotation, which can be verified by simple matrix multiplication:

$$\hat{Y}(\gamma) = e^{i(\pi-\gamma)} \hat{X}(\frac{3\pi}{2}) \hat{Z}(2\gamma) \hat{X}(\frac{\pi}{2}). \quad (\text{A3})$$

Substituting this into \hat{U}_{YZZ} and setting $\hat{U}_{YZZ} = T_{n,m}(\theta, \phi)$:

$$T_{n,m}(\theta, \phi) = e^{i(\frac{\phi}{2} + \pi - \gamma)} \hat{Z}(\beta) \left[\hat{X}(\frac{3\pi}{2}) \hat{Z}(2\gamma) \hat{X}(\frac{\pi}{2}) \right] \hat{Z}(\delta). \quad (\text{A4})$$

We can use PennyLane's `one_qubit_decomposition` and find that the angles (δ, γ, β) . β are calculated as follows:

$$\beta = \arg(U_{10}) - \arg(U_{00}) \stackrel{U=T_{n,m}(\theta, \phi)}{=} \phi - \phi = 0. \quad (\text{A5})$$

Therefore, the $\hat{Z}(\beta)$ gate is the identity matrix. We can determine $\delta = -\phi$, similarly as β and by setting $\theta = \gamma$ we can finally write

$$T_{n,m}(\theta, \phi) = e^{i(\frac{\phi-\theta}{2} + \pi)} \hat{X}(\frac{3\pi}{2}) \hat{Z}(2\theta) \hat{X}(\frac{\pi}{2}) \hat{Z}(-\phi) \quad (\text{A6})$$

As a last step, we convert the symmetric \hat{Z} gates into the asymmetric \hat{Z} gates defined in Eq. 1: We have $\hat{Z}_{sym}(\xi) = e^{-i\xi/2} \underbrace{\text{diag}(1, e^{i\xi})}_{Z_{\text{asym}}(\xi)}$. So we find

$$\alpha = \frac{\phi}{2} + \pi - \frac{\theta}{2} - \frac{\theta}{2} + \frac{\phi}{2} = \phi - \theta + \pi. \quad (\text{A7})$$

Appendix B: Absorption of Phase in Diagonal Matrix

The phase factors of the form $e^{i(\phi-\theta+\pi)}$ occurring in the Z_2X_2 decomposition can be moved through the gate sequence by permutation and be absorbed in an overall diagonal phase shift D . To see this, consider a unitary matrix U decomposed into $T_{n,m}$ building blocks, e.g. for $\dim(U) = 4$:

$$U = D \cdot T_{1,2}T_{2,3}T_{0,1}T_{1,2}T_{2,3}T_{0,1}. \quad (\text{B1})$$

Each of these $T_{n,m}$ can be decomposed into $T_{n,m} = S * P$ where $S \in SU(2)$ and $P = \text{diag}(e^{i\alpha}, e^{i\beta})$. Therefore, we

have

$$U = D \cdot (S_{1,2}P_{1,2})(S_{2,3}P_{2,3})(S_{0,1}P_{0,1})(S_{1,2}P_{1,2}) \\ (S_{2,3}P_{2,3})(S_{0,1}P_{0,1}). \quad (\text{B2})$$

For each $S_{n,m}P_{n,m}$ we can find $S'_{n,m}$ and $P'_{n,m}$ such that $S_{n,m}P_{n,m} = P'_{n,m}S'_{n,m}$. Therefore, we can rewrite Eq. B2 as

$$U = D \cdot (S_{1,2}P_{1,2})(S_{2,3}P_{2,3})(S_{0,1}P_{0,1})(S_{1,2}P_{1,2}P'_{0,1}) \\ (S_{2,3}P_{2,3})(S'_{0,1}) \quad (\text{B3})$$

since $P'_{0,1}$ commutes with $S_{2,3}P_{2,3}$. We can now combine $P_{1,2}P'_{0,1}$ into $P_{0,1,2}$. Now we repeat this and find $P'_{0,1,2}S'_{1,2}$ etc. until we end up at

$$U = D \cdot P_{0,1,2,3}S'_{1,2}S'_{2,3} \dots S'_{0,1} = D' \cdot S'_{1,2}S'_{2,3} \dots S'_{0,1} \quad (\text{B4})$$

-
- [1] M. A. Nielsen and I. L. Chuang, Quantum Computation and Quantum Information (1991).
- [2] A. Barenco, C. H. Bennett, R. Cleve, D. P. DiVincenzo, N. Margolus, P. Shor, T. Sleator, J. A. Smolin, and H. Weinfurter, Elementary Gates for Quantum Computation, Phys. Rev. A **52**, 3457 (1995).
- [3] M. Foss-Feig, G. Pagano, A. C. Potter, and N. Y. Yao, Progress in Trapped-Ion Quantum Simulation, Annual Review of Condensed Matter Physics **16**, 145–172 (2025).
- [4] M. Kjaergaard, M. E. Schwartz, J. Braumüller, P. Krantz, J. I.-J. Wang, S. Gustavsson, and W. D. Oliver, Superconducting Qubits: Current State of Play, Annual Review of Condensed Matter Physics **11**, 369–395 (2020).
- [5] M. Reck, A. Zeilinger, H. J. Bernstein, and P. Bertani, Experimental Realization of Any Discrete Unitary Operator, Phys. Rev. Lett. **73**, 58 (1994).
- [6] W. R. Clements, P. C. Humphreys, B. J. Metcalf, W. S. Kolthammer, and I. A. Walmsley, Optimal Design for Universal Multiport Interferometers, Optica **3**, 1460 (2016).
- [7] J. Wang, F. Sciarrino, A. Laing, and M. G. Thompson, Integrated Photonic Quantum Technologies, Nature Photonics **14**, 273–284 (2019).
- [8] C. Gross and I. Bloch, Quantum Simulations with Ultracold Atoms in Optical Lattices, Science **357**, 995–1001 (2017).
- [9] F. Schäfer, T. Fukuhara, S. Sugawa, Y. Takasu, and Y. Takahashi, Tools for Quantum Simulation with Ultracold Atoms in Optical Lattices, Nature Reviews Physics **2**, 411–425 (2020).
- [10] C. Tabares, C. Kokail, P. Zoller, D. González-Cuadra, and A. González-Tudela, Programming Optical-Lattice Fermi-Hubbard Quantum Simulators, PRX Quantum **6**, 030356 (2025).
- [11] A. R. Cavallar, L. Escalera-Moreno, T. Franz, T. Hilker, J. I. Cirac, P. M. Preiss, and B. F. Schiffer, Phase-Sensitive Measurements on a Fermi-Hubbard Quantum Processor (2025), arXiv:2509.01637.
- [12] A. J. Daley, H. Pichler, J. Schachenmayer, and P. Zoller, Measuring Entanglement Growth in Quench Dynamics of Bosons in an Optical Lattice, Phys. Rev. Lett. **109**, 020505 (2012).
- [13] H. Pichler, L. Bonnes, A. J. Daley, A. M. Läuchli, and P. Zoller, Thermal versus Entanglement Entropy: A Measurement Protocol for Fermionic Atoms with a Quantum Gas Microscope, New Journal of Physics **15**, 063003 (2013).
- [14] A. Impertro, S. Karch, J. F. Wienand, S. Huh, C. Schweizer, I. Bloch, and M. Aidelsburger, Local Readout and Control of Current and Kinetic Energy Operators in Optical Lattices, Physical Review Letters **133**, 063401 (2024).
- [15] H. Schlömer, H. Lange, T. Franz, T. Chalopin, P. Bojović, S. Wang, I. Bloch, T. A. Hilker, F. Grusdt, and A. Bohrdt, Local Control and Mixed Dimensions: Exploring High-Temperature Superconductivity in Optical Lattices, PRX Quantum **5**, 040341 (2024).
- [16] D. K. Mark, H.-Y. Hu, J. Kwan, C. Kokail, S. Choi, and S. F. Yelin, Efficiently Measuring d-Wave Pairing and Beyond in Quantum Gas Microscopes, Physical Review Letters **135**, 123402 (2025).
- [17] D. González-Cuadra, D. Bluvstein, M. Kalinowski, R. Kaubuegger, N. Maskara, P. Naldesi, T. V. Zache, A. M. Kaufman, M. D. Lukin, H. Pichler, B. Vermersch, J. Ye, and P. Zoller, Fermionic Quantum Processing with Programmable Neutral Atom Arrays, Proceedings of the National Academy of Sciences **120**, e2304294120 (2023).
- [18] F. Gkritis, D. Dux, J. Zhang, N. Jain, C. Gogolin, and P. M. Preiss, Simulating Chemistry with Fermionic Optical Superlattices, PRX Quantum **6**, 010318 (2025).
- [19] A. Schuckert, E. Crane, A. V. Gorshkov, M. Hafezi, and M. J. Gullans, Fault-Tolerant Fermionic Quantum Computing (2024), arXiv:2411.08955.
- [20] R. Ott, D. González-Cuadra, T. V. Zache, P. Zoller, A. M. Kaufman, and H. Pichler, Error-Corrected

- Fermionic Quantum Processors with Neutral Atoms, *Phys. Rev. Lett.* **135**, 090601 (2025).
- [21] W.-Y. Zhang, M.-G. He, H. Sun, Y.-G. Zheng, Y. Liu, A. Luo, H.-Y. Wang, Z.-H. Zhu, P.-Y. Qiu, Y.-C. Shen, X.-K. Wang, W. Lin, S.-T. Yu, B.-C. Li, B. Xiao, M.-D. Li, Y.-M. Yang, X. Jiang, H.-N. Dai, Y. Zhou, X. Ma, Z.-S. Yuan, and J.-W. Pan, Scalable Multipartite Entanglement Created by Spin Exchange in an Optical Lattice, *Phys. Rev. Lett.* **131**, 073401 (2023).
- [22] Z. Zhu, Y. Kiefer, S. Jele, M. Gächter, G. Bisson, K. Viebahn, and T. Esslinger, Splitting and Connecting Singlets in Atomic Quantum Circuits, *Phys. Rev. X* **15**, 041032 (2025).
- [23] T. Chalopin, P. Bojović, D. Bourgund, S. Wang, T. Franz, I. Bloch, and T. Hilker, Optical Superlattice for Engineering Hubbard Couplings in Quantum Simulation, *Physical Review Letters* **134**, 053402 (2025).
- [24] R. Islam, R. Ma, P. M. Preiss, M. Eric Tai, A. Lukin, M. Rispoli, and M. Greiner, Measuring Entanglement Entropy in a Quantum Many-Body System, *Nature* **528**, 77–83 (2015).
- [25] A. M. Kaufman and K.-K. Ni, Quantum Science with Optical Tweezer Arrays of Ultracold Atoms and Molecules, *Nature Physics* **17**, 1324–1333 (2021).
- [26] J. Sebby-Strabley, M. Anderlini, P. S. Jessen, and J. V. Porto, Lattice of Double Wells for Manipulating Pairs of Cold Atoms, *Phys. Rev. A* **73**, 033605 (2006).
- [27] M. Anderlini, P. J. Lee, B. L. Brown, J. Sebby-Strabley, W. D. Phillips, and J. V. Porto, Controlled Exchange Interaction Between Pairs of Neutral Atoms in an Optical Lattice, *Nature* **448**, 452–456 (2007).
- [28] S. Fölling, S. Trotzky, P. Cheinet, M. Feld, R. Saers, A. Widera, T. Müller, and I. Bloch, Direct Observation of Second-Order Atom Tunneling, *Nature* **448**, 1029–1032 (2007).
- [29] H.-N. Dai, B. Yang, A. Reingruber, H. Sun, X.-F. Xu, Y.-A. Chen, Z.-S. Yuan, and J.-W. Pan, Four-Body Ring-Exchange Interactions and Anyonic Statistics Within a Minimal Toric-Code Hamiltonian, *Nature Physics* **13**, 1195–1200 (2017).
- [30] P. Bojović, T. Hilker, S. Wang, J. Obermeyer, M. Barendregt, D. Tell, T. Chalopin, P. M. Preiss, I. Bloch, and T. Franz, High-Fidelity Collisional Quantum Gates with Fermionic Atoms (2025), arXiv:2506.14711.
- [31] Z. Zhu, Y. Kiefer, S. Jele, M. Gächter, G. Bisson, K. Viebahn, and T. Esslinger, Splitting and Connecting Singlets in Atomic Quantum Circuits (2025).
- [32] W. Bogaerts, D. Pérez, J. Capmany, D. A. B. Miller, J. Poon, D. Englund, F. Morichetti, and A. Melloni, Programmable Photonic Circuits, *Nature* **586**, 207–216 (2020).
- [33] J. M. Arrazola, V. Bergholm, K. Brádler, T. R. Bromley, M. J. Collins, I. Dhand, A. Fumagalli, T. Gerrits, A. Goussev, L. G. Helt, et al., Quantum Circuits with Many Photons on a Programmable Nanophotonic Chip, *Nature* **591**, 54 (2021).
- [34] Y. Xie, X. Ke, S. Hong, Y. Sun, L. Song, H. Li, P. Wang, and D. Dai, Complex-Valued Matrix-Vector Multiplication Using a Scalable Coherent Photonic Processor, *Science Advances* **11**, eads7475 (2025).
- [35] D. Pérez-López, A. Gutierrez, D. Sánchez, A. López-Hernández, M. Gutierrez, E. Sánchez-Gomáriz, J. Fernández, A. Cruz, A. Quirós, Z. Xie, et al., General-Purpose Programmable Photonic Processor for Advanced Radiofrequency Applications, *Nature Communications* **15**, 1563 (2024).
- [36] C. Robens, I. n. Arrazola, W. Alt, D. Meschede, L. Lamata, E. Solano, and A. Alberti, Boson Sampling with Ultracold Atoms in a Programmable Optical Lattice, *Phys. Rev. A* **110**, 012615 (2024).
- [37] M. Greiner, O. Mandel, T. Esslinger, T. W. Hänsch, and I. Bloch, Quantum Phase Transition from a Superfluid to a Mott Insulator in a Gas of Ultracold Atoms, *nature* **415**, 39 (2002).
- [38] G. Jotzu, M. Messer, R. Desbuquois, M. Lebrat, T. Uehlinger, D. Greif, and T. Esslinger, Experimental Realization of the Topological Haldane Model with Ultracold Fermions, *Nature* **515**, 237–240 (2014).
- [39] P. T. Brown, E. Guardado-Sanchez, B. M. Spar, E. W. Huang, T. P. Devereaux, and W. S. Bakr, Angle-Resolved Photoemission Spectroscopy of a Fermi-Hubbard System, *Nature Physics* **16**, 26–31 (2019).
- [40] M. Holten, L. Bayha, K. Subramanian, S. Brandstetter, C. Heintze, P. Lunt, P. M. Preiss, and S. Jochim, Observation of Cooper Pairs in a Mesoscopic Two-Dimensional Fermi Gas, *Nature* **606**, 287 (2022).
- [41] A. W. Glaetzle, K. Ender, D. S. Wild, S. Choi, H. Pichler, M. D. Lukin, and P. Zoller, Quantum Spin Lenses in Atomic Arrays, *Phys. Rev. X* **7**, 031049 (2017).
- [42] T. Olson, The Discrete Fourier Transform, *Applied Fourier Analysis: From Signal Processing to Medical Imaging*, 75 (2017).
- [43] C. Candan, M. A. Kutay, and H. M. Ozaktas, The Discrete Fractional Fourier Transform, *IEEE Transactions on signal processing* **48**, 1329 (2000).
- [44] G. Bentsen, T. Hashizume, A. S. Buyskikh, E. J. Davis, A. J. Daley, S. S. Gubser, and M. Schleier-Smith, Tree-like Interactions and Fast Scrambling with Cold Atoms, *Physical review letters* **123**, 130601 (2019).
- [45] D. Barredo, S. de Léséleuc, V. Lienhard, T. Lahaye, and A. Browaeys, An Atom-by-Atom Assembler of Defect-Free Arbitrary Two-Dimensional Atomic Arrays, *Science* **354**, 1021–1023 (2016).
- [46] A. W. Young, S. Geller, W. J. Eckner, N. Schine, S. Glancy, E. Knill, and A. M. Kaufman, An Atomic Boson Sampler, *Nature* **629**, 311–316 (2024).
- [47] F. Gyger, M. Ammenwerth, R. Tao, H. Timme, S. Snigirev, I. Bloch, and J. Zeiher, Continuous Operation of Large-Scale Atom Arrays in Optical Lattices, *Physical Review Research* **6**, 033104 (2024).
- [48] H. J. Manetsch, G. Nomura, E. Bataille, X. Lv, K. H. Leung, and M. Endres, A Tweezer Array with 6, 100 Highly Coherent Atomic Qubits, *Nature* **647**, 60–67 (2025).
- [49] D. Bluvstein, S. J. Evered, A. A. Geim, S. H. Li, H. Zhou, T. Manovitz, S. Ebadi, M. Cain, M. Kalinowski, D. Hangleiter, et al., Logical Quantum Processor Based on Reconfigurable Atom Arrays, *Nature* **626**, 58 (2024).
- [50] R. Lin, H.-S. Zhong, Y. Li, Z.-R. Zhao, L.-T. Zheng, T.-R. Hu, H.-M. Wu, Z. Wu, W.-J. Ma, Y. Gao, Y.-K. Zhu, Z.-F. Su, W.-L. Ouyang, Y.-C. Zhang, J. Rui, M.-C. Chen, C.-Y. Lu, and J.-W. Pan, AI-Enabled Parallel Assembly of Thousands of Defect-Free Neutral Atom Arrays, *Phys. Rev. Lett.* **135**, 060602 (2025).
- [51] S. A. Moses, C. H. Baldwin, M. S. Allman, R. Ancona, L. Ascarrunz, C. Barnes, J. Bartolotta, B. Bjork, P. Blanchard, M. Bohn, et al., A Race-Track Trapped-Ion Quantum Processor, *Physical Review X* **13**, 041052 (2023).
- [52] X. Wu, H. Yan, G. Andersson, A. Anferov, M.-H. Chou,

- C. R. Conner, J. Grebel, Y. J. Joshi, S. Li, J. M. Miller, et al., Modular Quantum Processor with an All-to-All Reconfigurable Router, *Physical Review X* **14**, 041030 (2024).
- [53] I. V. Dudinets, S. S. Straupe, A. K. Fedorov, and O. V. Lychkovskiy, All-to-All Connectivity of Rydberg-Atom-Based Quantum Processors with Messenger Qubits, arXiv preprint arXiv:2504.05087 (2025).
- [54] A. Kaufman, B. Lester, M. Foss-Feig, M. Wall, A. Rey, and C. Regal, Entangling Two Transportable Neutral Atoms via Local Spin Exchange, *Nature* **527**, 208 (2015).
- [55] W. Lechner, P. Hauke, and P. Zoller, A Quantum Annealing Architecture with All-to-All Connectivity from Local Interactions, *Science Advances* **1**, e1500838 (2015).
- [56] P. Pham and K. M. Svore, A 2D Nearest-Neighbor Quantum Architecture for Factoring in Polylogarithmic Depth, arXiv preprint arXiv:1207.6655 (2012).
- [57] D. J. Brod, E. F. Galvão, A. Crespi, R. Osellame, N. Spagnolo, and F. Sciarrino, Photonic Implementation of Boson Sampling: A Review, *Advanced Photonics* **1**, 034001 (2019).
- [58] S. A. Fldzhyan, M. Y. Saygin, and S. P. Kulik, Optimal Design of Error-Tolerant Reprogrammable Multiport Interferometers, *Optics Letters* **45**, 2632 (2020).
- [59] B. A. Bell and I. A. Walmsley, Further Compactifying Linear Optical Unitaries, *APL Photonics* **6**, 070804 (2021).
- [60] C. Arends, L. Wolf, J. Meinecke, S. Barkhofen, T. Weich, and T. J. Bartley, Decomposing Large Unitaries into Multimode Devices of Arbitrary Size, *Phys. Rev. Res.* **6**, L012043 (2024).
- [61] P. A. A. Yasir and P. van Loock, Compactifying Linear Optical Unitaries Using Multiport Beamsplitters (2025), arXiv:2505.11371.
- [62] M. C. Tichy, M. Tiersch, F. Mintert, and A. Buchleitner, Many-Particle Interference Beyond Many-Boson and Many-Fermion Statistics, *New Journal of Physics* **14**, 093015 (2012).
- [63] A. M. Childs and J. Goldstone, Spatial Search by Quantum Walk, *Phys. Rev. A* **70**, 022314 (2004).
- [64] Data is available at: <https://gitlab.mpcdf.mpg.de/mpq-fermiqp/constructing-arbitrary-coherent-rearrangements-in-optical-lattices/-/tree/main>.